

CL 316: Separation Process II

Report: Separation with a Centrifuge and Dryer

Pankaj [22110177]

Ankit [22110025]

Introduction

Separation and purification of solid crystals from liquid mixtures are fundamental operations in chemical, pharmaceutical, and food industries. Crystallization followed by solid-liquid separation and subsequent drying is a widely employed method to obtain purified solid products. Achieving efficient and complete separation requires selection of separation and drying technologies suited to the physical properties of the crystals and mother liquor. In this project, a sequential two-step process was simulated and analyzed using COMSOL Multiphysics: first, the separation of crystals from a slurry using a tubular centrifuge, and then the drying of these separated crystals using a vacuum dryer.

The centrifugal separation process ensures that solid crystals are rapidly and effectively separated from the surrounding liquid without damaging their structure, which is critical for maintaining product quality, especially for delicate or heat-sensitive crystals. Subsequently, the vacuum drying stage enables the removal of residual moisture at low temperatures and low pressures, preserving the integrity and stability of the final solid product. This sequential approach mirrors real industrial practices where centrifugation is often employed immediately after crystallization, followed by low-temperature drying. The primary objectives of this study are to model the centrifugal separation and vacuum drying processes, to examine how critical variables such as rotational speed, particle size, vacuum pressure, and temperature affect process performance, and to derive insights that would guide optimal process design and operation. By successfully simulating this sequential operation, we aim to deepen our understanding of how to maximize yield, maintain product quality, and minimize energy consumption in industrial-scale separation and drying processes.

Background Research

Tubular Centrifuge

A tubular centrifuge is a high-speed device used to separate solids from liquids based on their density difference. When a suspension is fed into the rotating chamber, solid particles experience a centrifugal force much higher than gravitational acceleration, causing rapid sedimentation toward the wall of the tube. The centrifugal force acting on a particle is defined as

$$F_c = m\omega^2 r$$

where, m is the particle mass, ω is the angular velocity, and r is the distance from the center of rotation.

The force exerted by a particle on a wall is defined as:

$$F_t = \frac{d(m_v v)}{dt}$$

where, F_t is the force, m is the particle mass, v is the velocity of a particle and t represents time. This equation expresses the rate of change of momentum ($m_v v$) with respect to time, which gives the force exerted by the particle on the wall.

The settling velocity v of a particle under centrifugal action can be given by

$$v = \frac{d_p^2(\rho_p - \rho_f)\omega^2 r}{18\mu}$$

where, d_p is the particle diameter, ρ_p and ρ_f are the densities of the particle and fluid respectively, and μ is the dynamic viscosity of the fluid. Tubular centrifuges are especially suitable for separating fine particles from dilute suspensions, offering advantages such as high throughput, continuous operation, and minimized mechanical damage to delicate crystals. Parameters such as rotational speed, particle size, feed flow rate, and viscosity of the liquid critically influence the efficiency of the separation process.

Vacuum Dryer

Vacuum drying is a thermal operation that removes moisture from solids at low temperatures by reducing the ambient pressure, thus lowering the boiling point of the liquid to be evaporated. This method is particularly useful for heat-sensitive materials where conventional drying could lead to thermal degradation. The fundamental principle relies on the difference in vapor pressure between the material surface and the vacuum environment, driving mass transfer in the form of evaporation. The drying rate can be expressed by a modified Fick's law:

$$\frac{dM}{dt} = -kA(P_v - P_{v0})$$

where, M is the moisture content, k is the mass transfer coefficient, A is the exposed surface area, P_v is the vapor pressure at the surface, and P_{v0} is the vapor pressure in the vacuum. By operating under vacuum, the process not only enhances drying rates but also preserves the structural and chemical integrity of the crystals, making it ideal for pharmaceuticals, fine chemicals, and high-value food ingredients.

Fourier's law of heat conduction to determine heat flow is given by:

$$\mathbf{q} = -k \nabla T$$

where, \mathbf{q} = Heat flux vector, k is thermal conductivity and ∇T is Gradient of temperature

In the vacuum drying model, we want to track how the total evaporation rate changes with time during the drying of the crystal Solid. The evaporation rate per unit volume \dot{m}_{LG} is already

defined in the model through the coefficient form PDE. To obtain the total evaporation rate (mass flow rate, kg/s), we integrate this local evaporation rate over the entire Solid domain. The total evaporation rate at a given time is calculated by:

$$\dot{M}(t) = \int_{\Omega} \dot{m}_{LG} dV$$

Where $\dot{M}(t)$ is the total mass evaporation rate at time t , \dot{m}_{LG} is local evaporation rate per unit volume, Ω is the volume of the drying Solid and dV is a volume element.

Overall Workflow

We aim to simulate and analyze a sequential separation and drying process for a mixture of three salt crystals suspended in water: Salt A, B, and C. These salts were specifically chosen because they represent a range of densities, providing a realistic challenge for separation: A with a high density, B with a medium density, and C with a lower density. Our overall approach mirrors an industrial sequence where separation and drying are performed one after another to isolate and preserve high-quality solid products efficiently.

The first stage involves using a tubular centrifuge to separate the salt crystals from the liquid phase based on their density differences. The centrifuge enables rapid and efficient separation by applying strong centrifugal forces that push the denser particles outward toward the tube walls, leaving clarified liquid near the center. A tubular centrifuge was specifically selected because of its high separation efficiency for fine particles, continuous operation, and ability to handle delicate crystals without significant mechanical damage. The cylindrical geometry ensures uniform radial acceleration, promoting better stratification of particles according to density.

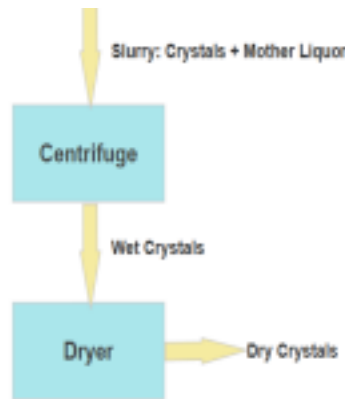


Figure 1: Schematic representation of flow

After separation, the second stage focuses on drying the collected salt crystals using a vacuum dryer. Vacuum drying is ideal for sensitive materials like crystals, as it enables moisture removal at lower temperatures by lowering the ambient pressure, thus minimizing the risk of thermal degradation. The vacuum dryer model was built in a 3D setup to capture the complex spatial

variation of moisture content and temperature inside the drying material. Choosing a 3D model instead of a 2D one allows us to better represent realistic industrial scenarios where heat and mass transfer occur in all directions within the drying Solid.

In the vacuum drying part of the study, several modules were built using varying operational parameters like space pressure, surface temperature, initial moisture content, and evaporation rate. By systematically altering these variables, we better understood how each parameter affects drying rate, surface temperature, and apparent moisture diffusivity when we vary the space pressure from 1000 Pa to 2000 Pa. The COMSOL models were designed to help us predict key outcomes such as drying time, moisture content profiles, temperature profiles, and total evaporation rates.

Through this sequential simulation, we seek to determine critical performance metrics. For the centrifuge stage, we aim to calculate separation efficiency, which is defined as the percentage of solids successfully separated from the liquid. For the drying stage, we are interested in plotting graphs of moisture content versus time, drying rate curves, and analyzing total drying times under different vacuum conditions and temperatures. These outputs will help us optimize process conditions for maximum efficiency and product quality.

Methodology

Tubular Centrifuge

In COMSOL Multiphysics, the Tubular Centrifuge model was set up using the manual Rotating Domain and Turbulent Flow physics modules. The geometry of the centrifuge was created in 3D, with a cylindrical tube having a height of 2.25 meters and a radius of 0.2 meters. A slurry containing three different density salts was introduced at the top inlet, where the flow velocity was controlled to simulate a typical feed condition.

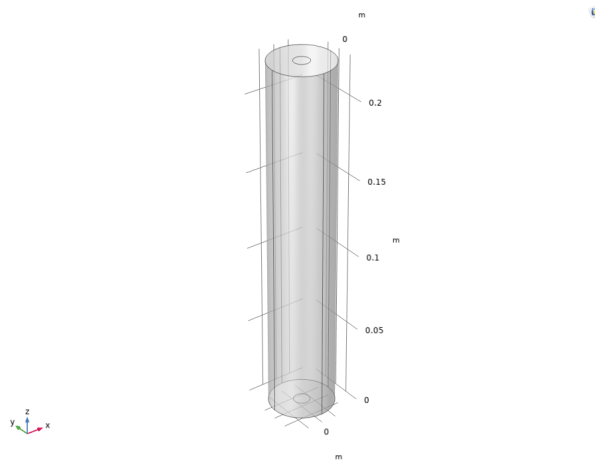


Figure 2: Geometry of tubular centrifugal

Physics modules:

The **Turbulent Flow**, **k- ω** and **Particle Tracing for Fluid Flow** physics interfaces were used. The Turbulent Flow k- ω model simulated the high-Reynolds-number flow inside the tubular centrifuge, capturing the turbulence near the walls. The Particle Tracing for Fluid Flow model was employed to track the motion of particles under the influence of centrifugal force, gravity, and drag. A rotating frame of reference was applied to generate the centrifugal effects needed for separation analysis.

Parameters:

Name	Expression	Value	Description
omega	1500[rad/s]	1500 rad/s	
L_tube	225[mm]	0.225 m	
R_tube	20[mm]	0.02 m	
R_feed	5[mm]	0.005 m	
Vol_f	2.5[l/min]	4.1667E-5 m ³ /s	
dia_part	20[um]	2E-5 m	
num_rel	1000	1000	
TIME	0[s]	0 s	

Table 1: Parameters of tubular centrifuge unit

The simulation parameters are defined as follows: the angular speed of the centrifuge, denoted by omega, is set to 1500 rad/s. The tube length (L_tube) is 0.225 meters, with a tube radius (R_tube) of 0.02 meters. The feed radius (R_feed) at the inlet is 0.005 meters. The fluid volumetric flow rate (Vol_f) is specified as 2.5 l/min, equivalent to 4.1667×10^{-5} m³/s. Particles introduced into the system have a diameter(dia_part) of 20 μm (2×10^{-5} meters). Furthermore, 2000 particles per type (num_rel) are released into the flow for the separation study.

Boundary conditions:

Inlet: A velocity inlet for the slurry with a defined flow rate and particle concentration.

Outlet: An open outlet at the base of the centrifuge to allow the clarified liquid to exit.

Walls: No-slip boundary condition applied to the internal surface of the tube, where solid particles settle due to centrifugal force.



Figure 3: Inlet (left) and Outlet (right) of the tubular centrifuge (green surface shown)

Mesh generational:

For mesh generation, a Normal boundary layer mesh was used to accurately resolve the steep velocity gradients near the wall and particle migration.

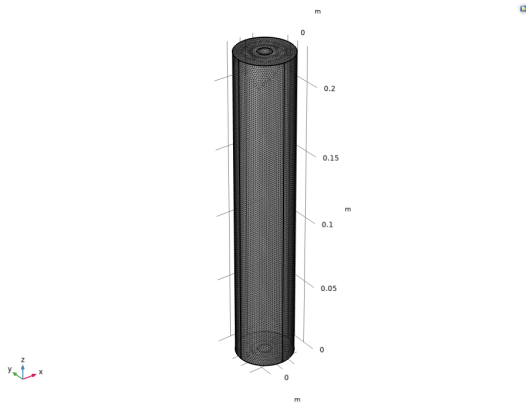


Figure 4: Mesh of the tubular centrifuge

Vacuum Dryer

In the vacuum drying model, the geometry represents a cylindrical container in a Nutsche filter dryer. Initially modeled in 2D axisymmetric coordinates, it consists of a cylindrical drum filled with a wet powder layer. It is exposed to vacuum at the top surface and heated along the side and bottom walls. The Dryer has a radius of 40 cm and a height of 10 cm, providing a relatively flat but thick slab of material for drying. In the updated 3D model, although the overall shape becomes fully three-dimensional, the physical setup remains the same — vacuum-assisted solvent evaporation occurs from the top surface. At the same time, conductive heating drives moisture migration from the interior toward the boundaries, enabling efficient low-pressure drying of the wet solid particles.

Physics modules:

The Vacuum Dryer setup in COMSOL utilized the Heat Transfer in Solids and Transport of Diluted Species modules to simulate the drying process. A 2D axisymmetric model was created to represent a thin slab of wet crystals inside a vacuum chamber. The initial moisture content of the material was set at 30% by weight. The Heat Transfer in Solids module modeled the temperature distribution in the material, while the Transport of Diluted Species module was used to simulate the mass transfer of moisture from the surface of the material to the surrounding vacuum environment.

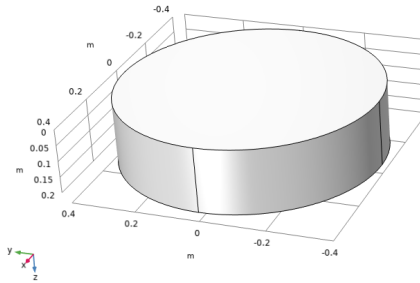


Figure 5: Geometry of the vacuum dryer

Parameters:

Parameters			
Name	Expression	Value	Description
A	5.31384	5.3138	Constant in Antoine equ...
alpha	1e-6[m^2/s]	1E-6 m^2/s	Proportionality constant...
B	1690.864[K]	1690.9 K	Constant in Antoine equ...
C	-51.804[K]	-51.804 K	Constant in Antoine equ...
CpG	1[J/(kg*K)]	1000 J/(kg·K)	Specific heat capacity, gas
CpL	4.18[J/(kg*K)]	4180 J/(kg·K)	Specific heat capacity, liq...
CpS	1800[J/(kg*K)]	1800 J/(kg·K)	Specific heat capacity, so...
deltaH	9720[cal/mol]/Mn	2.2575E6 J/kg	Latent heat of vaporizatio...
H0	20[cm]	0.2 m	Dryer length
hq	20[W/(m^2*K)]	20 W/(m^2·K)	Wall heat transfer coeffici...
kvap	1e-6[1/s]	1E-6 1/s	Evaporation rate constant
lambda_dry	0.2[W/(m^K)]	0.2 W/(m·K)	Effective thermal conduc...
lambda_w...	0.6[W/(m^K)]	0.6 W/(m·K)	Effective thermal conduc...
Mn	18.015[g/mol]	0.018015 kg/...	Molar mass (updated for...
pG	15[mbar]	1500 Pa	Head-space pressure
R0	40[cm]	0.4 m	Cake radius
rhoG	1[kg/m^3]	1 kg/m^3	Density, gas
rhoL	1000[kg/m^3]	1000 kg/m^3	Density, liquid (updated)
rhoS	1200[kg/m^3]	1200 kg/m^3	Density, solid (updated)
T0	20[degC]	293.15 K	Initial temperature
Th	60[degC]	333.15 K	Jacket temperature
thetal_star	0.05	0.05	Residual saturation
thetaS	0.7	0.7	Solid phase volume fracti...
wL0	0.20	0.2	Initial moisture content

Table 2: Parameters of vacuum dryer unit

In the updated model parameters, several material properties were changed to reflect a more realistic vacuum drying scenario involving water and a generic dry solid, like Salt Crystals. The liquid density ρ_L was updated to 1000 kg/m^3 , assuming the liquid phase behaves like pure water or an aqueous solution, which is common in vacuum drying processes. The solid density ρ_S was set to 1200 kg/m^3 , representing typical values for dry powders such as food or pharmaceutical materials. The liquid specific heat capacity $C_p L$ was updated to $4.18 \text{ kJ/(kg}\cdot\text{K)}$, matching that of water, which has a high heat capacity due to its ability to absorb significant amounts of heat with little temperature change. The solid specific heat capacity $C_p S$ was adjusted to $1800 \text{ J/(kg}\cdot\text{K)}$, a reasonable value for dry solids like polymers or starches.

The wet thermal conductivity λ_{wet} was set to $0.6 \text{ W/(m}\cdot\text{K)}$ because water has relatively high thermal conductivity, and in the wet solid region, water dominates the heat transfer behavior. The dry thermal conductivity λ_{dry} was updated to $0.2 \text{ W/(m}\cdot\text{K)}$, appropriate for dry porous solids, which are generally poor conductors of heat. The molar mass M_n was changed to 18.015 g/mol to represent water vapor, the primary substance evaporating during drying. Finally, the latent heat of vaporization ΔH , was slightly adjusted to 9720 cal/mol divided by M_n , aligning with the typical range for water vaporization under vacuum conditions. These updates ensure that the model more accurately reflects the physical behavior of typical drying processes.

Boundary conditions:

Surface of the material: A convective heat flux condition for heat transfer from the drying air to the material's surface, which was coupled with a mass flux condition for moisture removal. The evaporation rate was governed by the difference in vapor pressures between the material surface and the vacuum environment.

Vacuum Chamber Walls: Insulated boundaries were used to prevent heat loss from the chamber walls.

Outlet: A low-pressure outlet was applied to simulate the removal of evaporated moisture from the vacuum.

Mesh generational:

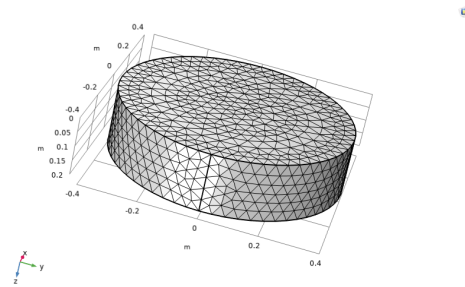


Figure 6: Mesh for the vacuum dryer

In terms of mesh generation, a fine mesh was used near the surface of the material to capture the steep temperature and moisture gradients during the drying process. The mesh was coarser away from the surface to reduce computational cost, but enough refinement was maintained to capture

the drying process accurately. The time-dependent study allowed the simulation of the drying process over time, and the results were used to calculate the drying time and moisture content as a function of time.

Results and Discussion

Tubular Centrifuge

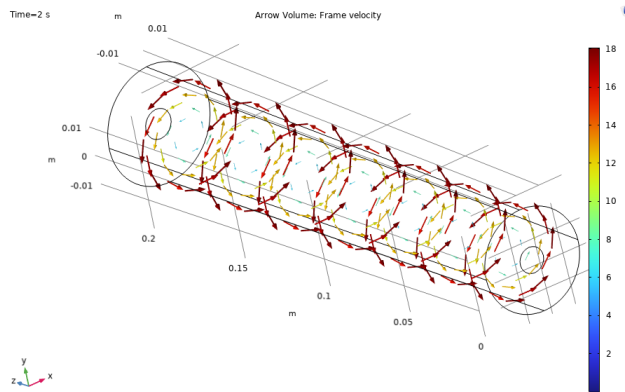


Figure 7: Velocity field representation in the rotating frame of reference

The fluid moves helically along the centrifuge wall due to the combined effect of rotation and axial flow. Higher velocities are observed near the walls, aiding in particle migration toward the cylinder boundary.

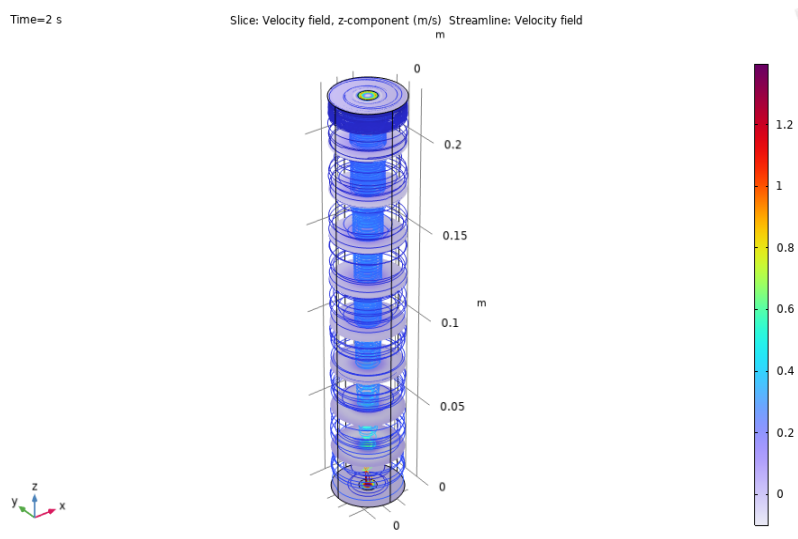


Figure 8: Velocity field and streamlines for the fluid flow

The velocity near the inlet's center is higher when the flow is completely developed. The fluid velocity in the axial direction drops right after the inlet due to the abrupt expansion in the geometry. The streamlines clearly show the impact of rotation. Also, near the walls, the velocity is lower due to the no-slip condition, while towards the center, the fluid moves faster.

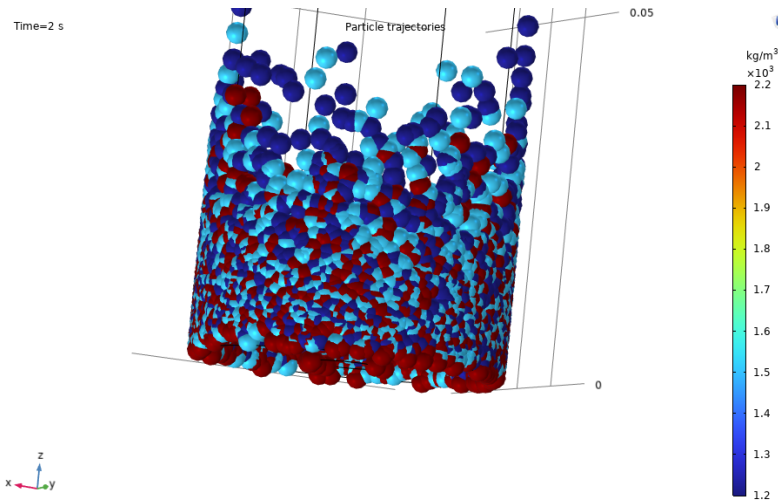


Figure 9: Particle trajectories based on densities

Centrifugal forces push the particles toward the cylinder walls, while the fluid flow carries them toward the outlet. Less dense particles are transported farther by the flow, whereas denser particles settle more quickly and accumulate near the inlet. Ideally, near the outlet, a significant concentration of the lowest-density particles should be observed. However, in this case, the particle trajectories do not match the expected behavior. This discrepancy arises because the rotating domain feature is not available in the COMSOL 6.1 version used in the labs. As a result, we added manual rotating domain, which did not produce highly accurate results.

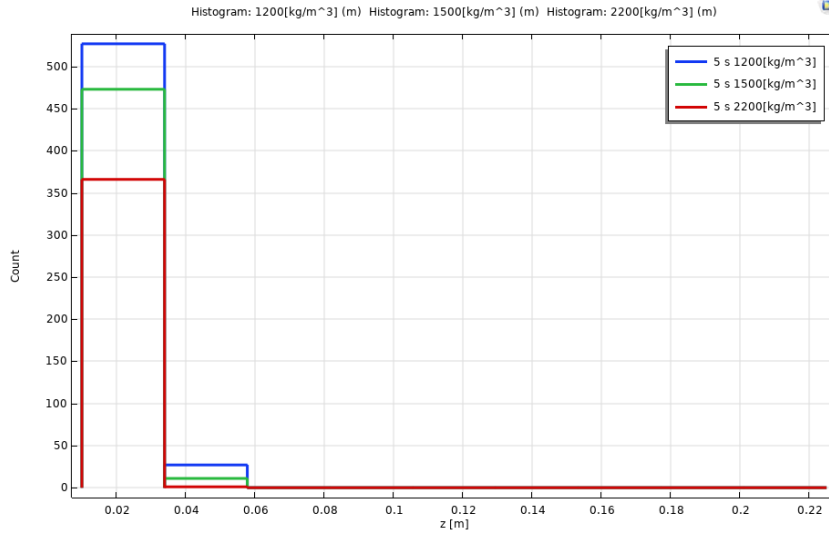


Figure 10: Distribution of particle densities collected at the wall as a function of the z-coordinate.

Initially, near the inlet, we expect the highest concentration of high-density particles, followed by medium-density particles, and the lowest count for low-density particles, as the heavier particles tend to deposit first. Similarly, at higher positions along the z-axis (near the outlet), we would expect the concentration of low-density particles to be the highest. However, contrary to these expectations, the simulation results do not show this clear trend, and a different distribution pattern is observed in the plot. The reason is again the non availability of the rotating domain.

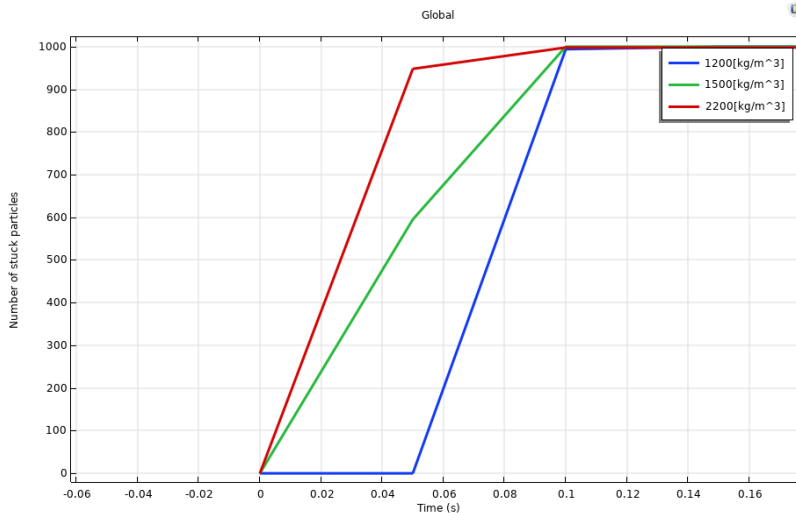


Figure 11 : Number of sedimented particles as a function of time

In the plot, we can observe that as time progresses, the number of high-density particles adhering to the wall initially increases rapidly. However, after a certain point, when most of the high-density particles have already settled, the rate of their accumulation slows down. Meanwhile, the lower-density particles begin to stick to the wall more noticeably. This behavior occurs because the higher-density particles settle first at the bottom, allowing the fluid

flow to carry the lower-density particles upward, where they eventually adhere to the wall at higher levels.

Efficiency:

Mean deposition height of class i is given by :

$$\bar{z}_i = \frac{1}{N_i} \sum_{k=1}^{N_i} z_{i,k}$$

where, $z_{i,k}$ is the axial coordinate where particle k of class i freezes, and N_i is the total number of particles injected for that class.

Pairwise separation efficiency between class i and j:

$$n_{i,j} = \frac{\bar{z}_j - \bar{z}_i}{L_{tube}} \times 100\%$$

Using this formula by finding sum of all freezed z in COMSOL in a density range we can get the average height, by using that we got these efficiencies:

A,B - 3.11 %

B,C - 3.19 %

C,A - 6.22 %

Where A is the highest density particle and C is the lowest density particle.

As we can observe that the A and C pair have the highest efficiency as they have the highest and lowest densities, hence a bigger gap, so easy separation.

So, overall we didn't get very accurate results from tubular centrifuge due to non availability of COMSOL 6.3. But still we did a detailed analysis on it. We also expected to assemble this to vacuum dryer via LiveLink for further purification of solid crystals. But as we didn't get accurate results and also there is non-availability of LiveLink in COMSOL 6.1, we analysed the dryer separately and we plan to assemble them in future.

Vacuum Dryer

Initially we varied the pressure and carried out detailed analysis on evaporation rates, moisture, temperature. We took three different pressure values: 1000 Pa., 1500 Pa and 2000 Pa.

Pressure = 1000 Pa

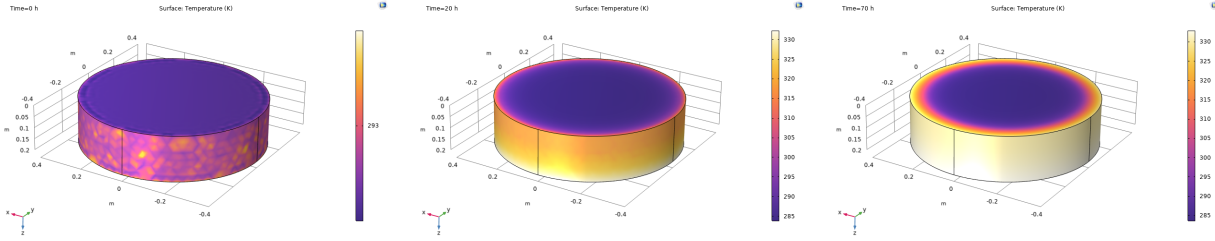


Figure 12: Surface temperature for pressure as 1000 Pa at time = 0 hours(left), 20 hours (middle), and 70 hours(right)

The surface temperature profiles at different times show that initially, the temperature is uniformly low across the surface. As drying progresses, the temperature increases, especially at the surface exposed to the vacuum. After 70 hours, the surface reaches a much higher temperature due to the reduced moisture content, which decreases evaporative cooling. This trend reflects effective heat transfer under low pressure conditions. As we can see the temperature at boundaries always remains high because it is direct in contact with the heating jacket.

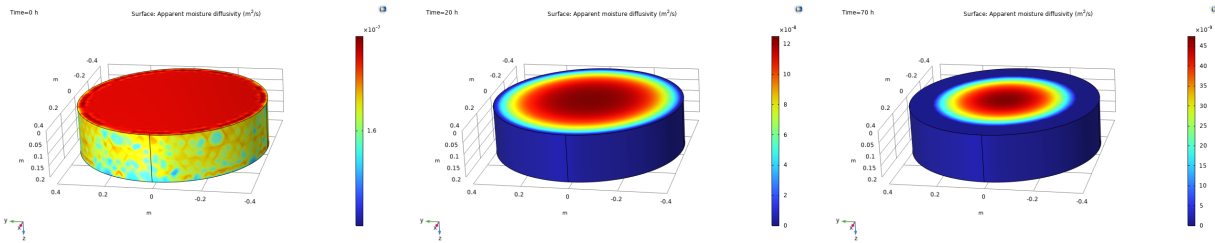


Figure 13 : Apparent moisture diffusivity for pressure as 1500 Pa at time = 0 hours(left), 20 hours (middle) and 70 hours(right)

The apparent moisture diffusivity decreases significantly over time. Initially, when the moisture content is high, diffusivity is higher due to easier moisture migration. As drying progresses and the material becomes drier, the moisture movement becomes more restricted, resulting in lower diffusivity values. Boundary moisture migration is higher than any other part as direct contact with the heating jacket.

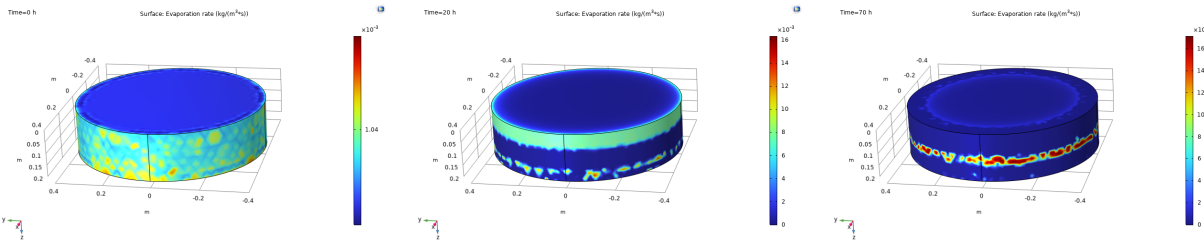


Figure 14: Evaporation rate for pressure as 1000 Pa at time = 0 hours(left), 20 hours (middle) and 70 hours(right)

The evaporation rate is highest at the beginning due to the large amount of free moisture available and decreases over time. As the surface dries and moisture has to diffuse from deeper layers, the evaporation rate drops, confirming the expected two-stage drying behavior: a constant rate period followed by a falling rate period.

Pressure = 1500 Pa

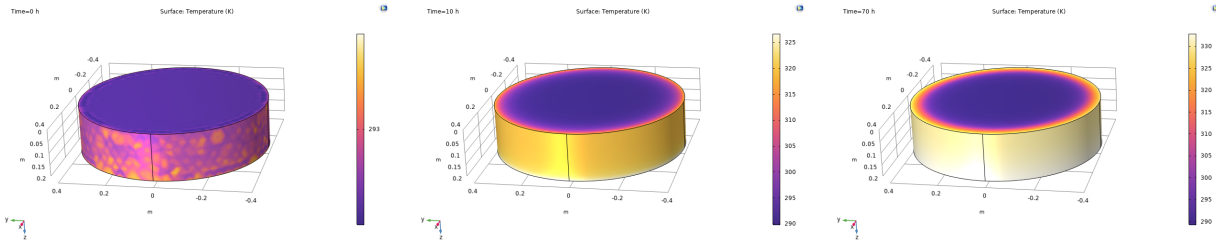


Figure 15: Surface temperature for pressure as 1500 Pa at time = 0 hours(left), 20 hours (middle), and 70 hours(right)

Similar to the 1000 Pa case, the surface temperature increases over time but slightly slower due to the higher ambient pressure, which reduces the evaporation cooling effect more slowly compared to deeper vacuum conditions.

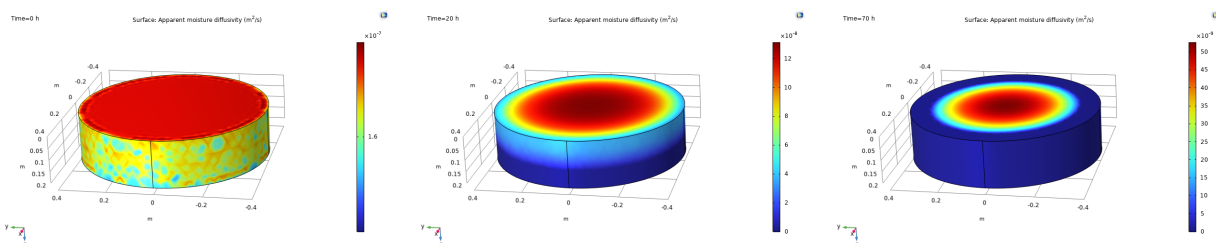


Figure 16: Apparent moisture diffusivity for pressure as 1500 Pa at time = 0 hours(left), 20 hours (middle), and 70 hours(right)

The diffusivity values at 1500 Pa also decrease over time, but remain slightly higher than in the 1000 Pa case at similar time points. This suggests that moisture migration is easier under a less deep vacuum, but overall drying is slower.

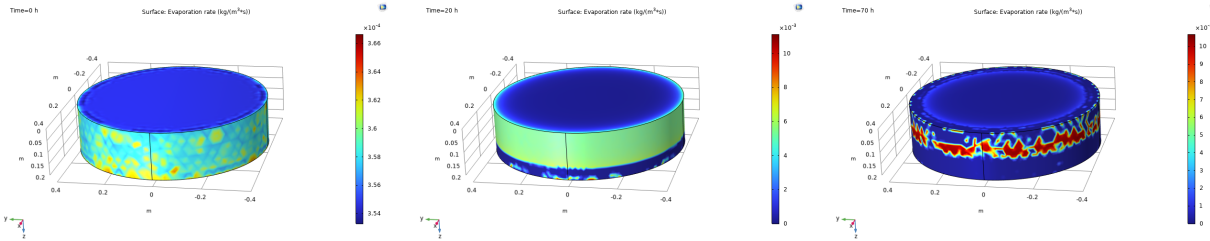


Figure 17 : Evaporation rate for pressure as 1500 Pa at time = 0 hours(left), 20 hours (middle) and 70 hours(right)

The evaporation rate starts high and declines, similar to the 1000 Pa scenario, but the initial evaporation rate is lower compared to 1000 Pa. This is due to the higher ambient pressure reducing the vapor pressure gradient, thereby slowing down evaporation.

Pressure = 2000 Pa

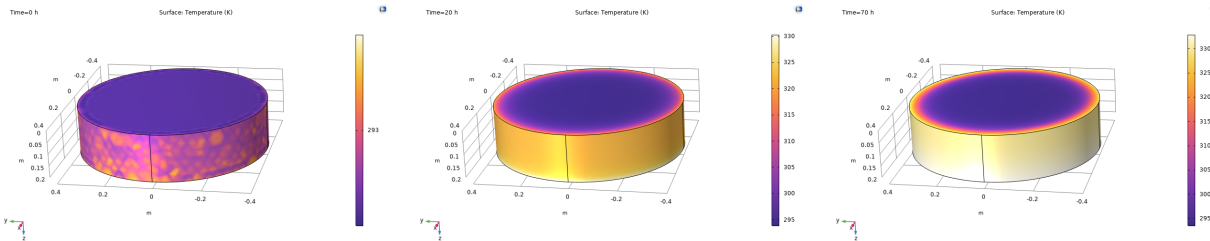


Figure 18 : Surface temperature for pressure as 2000 Pa at time = 0 hours(left), 20 hours (middle) and 70 hours(right)

At 2000 Pa, the surface temperature rise is slower and less pronounced, indicating that higher ambient pressure reduces both evaporation and heating rates. It takes much longer for the surface to reach a high temperature compared to deeper vacuum conditions.

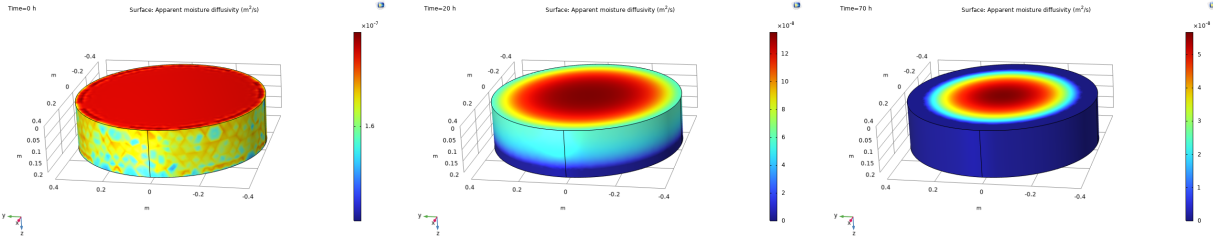


Figure 19 : Surface temperature for pressure as 2000 Pa at time = 0 hours(left), 20 hours (middle) and 70 hours(right)

The diffusivity drops over time here as well, but remains higher than both the 1000 Pa and 1500 Pa cases at early stages. However, overall drying is less efficient because lower evaporation reduces the driving force for mass transfer.

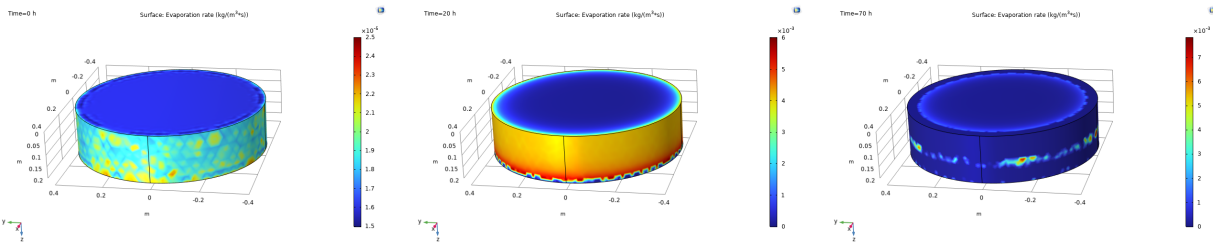


Figure 20 : Evaporation rate for pressure as 2000 Pa at time = 0 hours(left), 20 hours (middle) and 70 hours(right)

The evaporation rate is significantly lower at 2000 Pa than at lower pressures. This confirms that higher space pressures slow down drying, necessitating longer drying times or higher temperatures for achieving similar moisture removal.

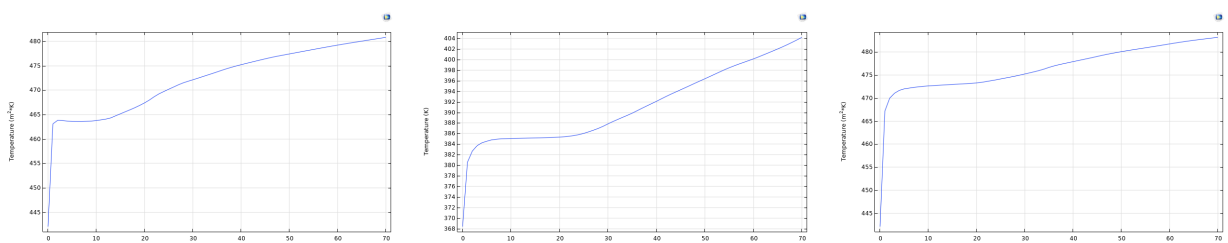


Figure 21 : Temperature vs time plots for different pressures conditions, 1000 Pa (left), 1500 Pa (middle) and 2000 Pa (right)

The plots show that lower pressure conditions (1000 Pa) allow the surface temperature to rise faster, while higher pressures delay temperature increase. This is due to the stronger evaporative cooling effect at lower pressures, which initially holds the surface temperature down but allows faster overall drying.

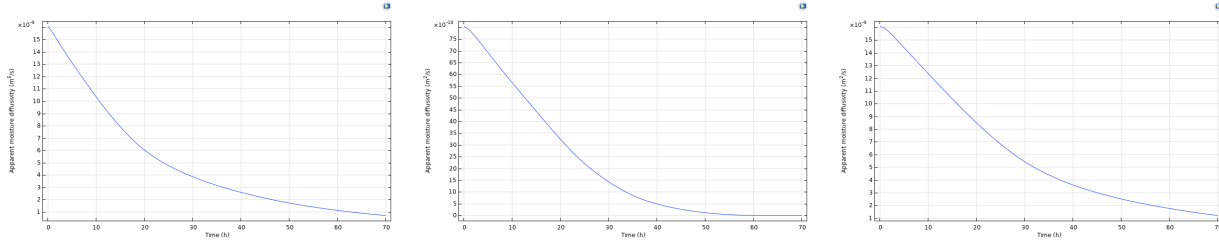


Figure 22 : Apparent moisture diffusivity vs time plots for different pressure conditions, 1000 Pa (left), 1500 Pa (middle) and 2000 Pa (right)

Moisture diffusivity decreases fastest for 1000 Pa, showing that the material dries quicker under deeper vacuum. For 1500 Pa and 2000 Pa, diffusivity remains higher for longer, indicating slower drying rates.

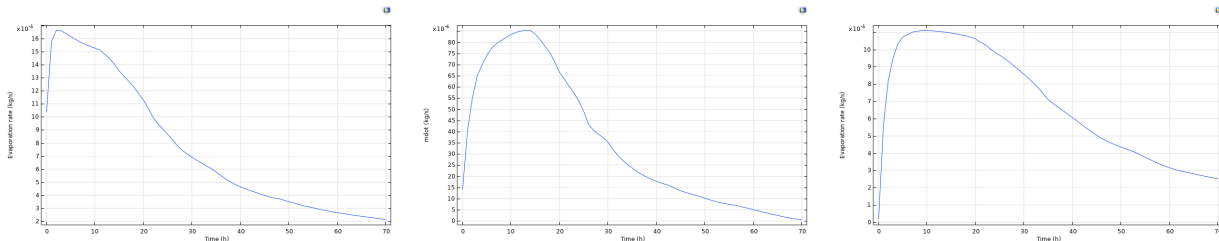


Figure 23 :Evaporation rate vs time plots for different pressure values,1000 Pa (left), 1500 Pa (middle) and 2000 Pa (right)

Evaporation rate starts higher and falls faster under deeper vacuum (1000 Pa) compared to higher pressures. This confirms that deeper vacuum accelerates drying by promoting faster moisture removal due to a greater vapor pressure differential.

Analyzed for three different head-space pressures: 1000 Pa, 1500 Pa, and 2000 Pa. All graphs show a similar pattern: an initial rapid rise in evaporation rate due to external heat transfer, reaching a peak between 5 and 10 hours, followed by a gradual decline as drying becomes limited by internal solvent diffusion. The evaporation driving force is determined by the difference between the equilibrium vapor pressure $P^*(T)$ and the head-space pressure P^G , i.e.,

$$\Delta P = P^*(T) - P^G$$

where, $P^*(T)$ is equilibrium vapor pressure at the material's surface (depends on temperature) and P^G is surrounding head-space pressure (vacuum).

Lower head-space pressure increases this driving force, accelerating evaporation

At 1000 Pa, the highest peak evaporation rate (1.6×10^{-5} kg/s) was observed, followed by slightly lower rates at 2000 Pa and 1500 Pa. This indicates that lower vacuum pressures (higher vacuum levels) significantly improve drying rates. Ranking the drying efficiency based on peak evaporation rates gives: 1000 Pa > 2000 Pa > 1500 Pa. Thus, applying a stronger vacuum improves overall drying performance by enhancing the evaporation rate and reducing the total drying time.

Efficiency under 1000 Pa is 12.24%

Efficiency under 1500 Pa is 4.424%

Efficiency under 2000 Pa is 3.96%

As we can see that lower vacuum pressure increases the efficiency as Lower pressure increases the evaporation driving force, reduces the boiling point, minimizes heat losses, and speeds up drying all leading to higher efficiency

Conclusion

We used COMSOL models to understand how centrifugal force and vacuum-driven evaporation work in concert to isolate and dehydrate salt crystals, but also exposed critical gaps between idealized simulations and real-world performance. In the centrifuge module, we visualized clear trends in particle trajectories denser crystals settling rapidly near the inlet and lighter ones migrating toward the outlet but manual rotating domain approach in COMSOL 6.1 capped pairwise separation efficiencies far below expected. In the dryer module, head-space pressures of 1000 Pa, 1500 Pa, and 2000 Pa produced distinct drying profiles: the deepest vacuum (1000 Pa) yielded the highest peak evaporation rate (1.6×10^{-5} kg/s) and a 12.2 % process efficiency, while shallower vacuum slowed both heat transfer and moisture diffusion. Key limitations include the inability to integrate centrifuge and dryer stages via LiveLink, the assumption of uniform 20 μm particle diameters and constant feed conditions, and the absence of any experimental or pilot-scale validation. **Future work** must leverage COMSOL 6.3's native rotating-domain and LiveLink capabilities to create fully coupled, dynamic simulations; incorporate a realistic particle-size distribution and variable feed rates; and benchmark model predictions against lab- or plant-scale trials. Only by bridging simulation with experimental data and optimizing energy-use metrics can we refine process parameters, reduce drying times, and scale these insights to commercial separation and drying operations.

References

- [1] "Centrifuge," Encyclopedia Britannica. [Online]. Available: <https://www.britannica.com/technology/centrifuge>. [Accessed: 27-Apr-2025].

[2] "Vacuum Drying," ScienceDirect. [Online]. Available: <https://www.sciencedirect.com/topics/agricultural-and-biological-sciences/vacuum-drying>. [Accessed: 27-Apr-2025].

[3] "Drying," Busch Vacuum Solutions. [Online]. Available: <https://www.buschvacuum.com/in/en/applications/drying/>. [Accessed: 27-Apr-2025].

[4] "Tubular Centrifuge," COMSOL. [Online]. Available: <https://www.comsol.com/model/tubular-centrifuge-127971>. [Accessed: 27-Apr-2025].

[5] "Vacuum Drying," COMSOL. [Online]. Available: <https://www.comsol.com/model/vacuum-drying-42561>. [Accessed: 27-Apr-2025].